

## Strength Characteristics and Electrochemical Impedance Spectroscopy Characterization of Red Mud–Coal Metakaolin Geopolymers

Jianping Liu<sup>1</sup>, Yisi Lu<sup>1</sup>, Xiaohong Bai<sup>1,2,\*</sup>, Pengju Han<sup>1</sup>, Ruizhen Xie<sup>3</sup>, Bin He<sup>1,4</sup>

<sup>1</sup> College of Civil Engineering, Taiyuan University of Technology, Taiyuan 030024, China

<sup>2</sup> Key Laboratory of Geotechnical and Underground Engineering of Shanxi Province, Taiyuan 030024, China

<sup>3</sup> Mechanics Institute, Jinzhong University, Taiyuan 030619, China

<sup>4</sup> State Key Laboratory of Geomechanics and Geotechnical Engineering, Institute of Rock and Soil Mechanics, Chinese Academy of Sciences, Wuhan, 430071, China

\*E-mail: [bxhong@tyut.edu.cn](mailto:bxhong@tyut.edu.cn)

Received: 16 July 2020 / Accepted: 31 August 2020 / Published: 30 September 2020

---

In this paper, the compressive strength and electrochemical impedance spectroscopy (EIS) of red mud–coal metakaolin (RM–CMK) geopolymers with different Na/Al atomic molar ratios at the age of 28 d were tested and analyzed. The Na/Al atomic molar ratio had significant influence on the compressive strength and EIS of the RM–CMK geopolymers. With increasing Na/Al, the compressive strength of the RM–CMK geopolymer first increased and then decreased. When Na/Al was 1.0, the compressive strength reached the maximum. The EIS results yielded a Nyquist diagram that presented flat capacitive reactance arcs in the high-frequency region and insignificant diffusion curves in the low-frequency region. The Bode diagram showed that with increasing Na/Al, the peak values of the impedance modulus and phase angle both first increased and then decreased. When Na/Al was 1.0, the peak values of the impedance modulus and phase angle reached the maximum. Combined with the variation law of EIS, the equivalent circuit of the RM–CMK geopolymer was determined to be  $R_e(C(R_{ct}W))$ . In addition, by means of a scanning electron microscope (SEM), images of the RM–CMK geopolymer microstructure were obtained. The changes in the strength and electrochemical responses of the RM–CMK geopolymer were explained from the microscopic perspective. In this study, EIS was used to test and analyze the electrochemical impedance characteristics of the geopolymer. This proved the feasibility of the application of EIS technology to geopolymer strength analysis. It also provided new ideas and means for the nondestructive testing technology of geopolymers.

---

**Keywords:** geopolymer, compressive strength, EIS, microstructure, equivalent circuit

## 1. INTRODUCTION

Red mud (RM) is an industrial waste residue produced during the production of alumina that is red because it contains a large amount of  $\text{Fe}_2\text{O}_3$  [1, 2]. Approximately 1.0-1.8 tons of red mud are produced for each ton of alumina produced by the Bayer process [3, 4]. China is one of the world's largest producers of red mud, with an annual output of up to one million tons. The global accumulation of red mud has exceeded 2.7 billion tons [5]. At present, red mud is mainly treated by dam storage and wet and dry storage methods. These methods not only occupy a large amount of land but also pollute the environment. However, due to the high contents of  $\text{SiO}_2$  and  $\text{Al}_2\text{O}_3$  in red mud, red mud has the main components needed to prepare geopolymers and has high alkalinity [6, 7]. Therefore, the use of red mud to replace silicate minerals to prepare geopolymers has attracted wide attention.

Coal metakaolin (CMK) is an amorphous aluminosilicate mineral formed by calcination and dehydration of coal kaolin. In the process of calcination, when the calcination temperature reaches 550-950 °C, the structural water is removed from coal kaolin [8, 9]. The  $\text{Al}^{3+}$  in the Al-OH octahedron diffuses and rearranges to form the Al-O bond, changing from six coordination to four coordination. The four coordination forms coal metakaolin, giving the material good pozzolanic activity [10, 11]. In terms of chemical composition, coal metakaolin is a mixture of  $\text{SiO}_2$  and  $\text{Al}_2\text{O}_3$  with chemical reactivity under normal temperature and pressure [12, 13]. At present, coal metakaolin is widely used in building materials, mainly to improve the working performance of cement-based materials and in the preparation of geopolymer materials.

Geopolymer is an amorphous aluminosilicate gelling material prepared from solid aluminosilicates excited by alkali metal hydroxides or silicate solutions, including silica tetrahedral prepared from natural minerals or solid waste [14, 15]. Amorphous and quasi-crystalline inorganic cementitious materials are formed by the polymerization of silicon oxygen tetrahedrons and aluminum oxide tetrahedrons [16, 17]. Compared to ordinary Portland cementitious materials, geopolymers have the characteristics of high early strength, good impermeability, high temperature resistance, good heat insulation effect, and strong corrosion resistance [18]. This material is a kind of environmentally friendly cement. In addition, geopolymers have the advantages of simple production processes, rich sources of raw materials (such as metakaolin, red mud, fly ash, and slag), low energy consumption and low environmental pollution (basically producing no emissions of  $\text{CO}_2$ ). Therefore, geopolymers have wide application prospects in the fields of the rapid repair of roads, solidification of waste materials and preparation of refractory materials.

Electrochemical impedance spectroscopy (EIS) is an important tool for studying the mechanical properties, microstructures and chemical reaction mechanisms of materials [19-23]. By using a small amplitude sinusoidal current as a disturbance signal, EIS can produce a response with an approximate linear relationship [24, 25]. Many scholars use EIS to study the physical properties, mechanical properties and durability of building materials. Zhang et al. studied the hydration process of cement through EIS and found that the early mechanism of the cement hydration process can be obtained from AC impedance spectroscopy [26]. Li et al. studied the compaction characteristics of loessial silt through EIS and found that EIS can reflect the compactness of loess-filled soil [27]. Zhang et al. studied a sandy soil system by EIS and established an equivalent circuit to analyze the effects of particle size and water

content on the equivalent circuit parameters [28]. Han et al. studied the mechanical properties of acidic and alkaline silty soils and the electrochemical corrosion behavior of X70 steel in H<sub>2</sub>SO<sub>4</sub> polluted silty soils through EIS [29, 30]. However, there are few reports on the use of EIS to study the mechanical properties of geopolymers.

In this study, the compressive strength and EIS of red mud–coal metakaolin (RM–CMK) geopolymer under different Na/Al atomic molar ratios were tested. The effects of the Na/Al atomic molar ratio on the compressive strength and EIS of the RM–CMK geopolymer were analyzed. Combined with the variation law of EIS, the equivalent circuit of the RM–CMK geopolymer was established. The equivalent circuit parameters were analyzed by ZsimpWin software. In addition, by means of a scanning electron microscope (SEM), images of the RM–CMK geopolymer microstructure were obtained. The changes in the strength and electrochemical response of the RM–CMK geopolymer were explained from the microscopic perspective.

## 2. EXPERIMENTAL PROCEDURE

### 2.1 Experimental materials

#### 2.1.1 RM

Bayer red mud was obtained from Shanxi Hejin Aluminum Co., Ltd. After the red mud raw material was crushed, a particle separation test was carried out to ensure that particles sized smaller than 75  $\mu\text{m}$  (200 mesh) accounted for more than 90% of the total mass. Table 1 lists the physical parameters. Table 2 lists the chemical composition. Fig. 1(a) shows an SEM image of the RM.

#### 2.1.2 CMK

CMK used in this study was commissioned by Shanxi Jinyu Kelin Technology Co., Ltd. Particles sized smaller than 2  $\mu\text{m}$  (6250 mesh) accounted for more than 90% of the total mass. Table 3 lists the chemical composition. Fig. 1(b) shows an SEM image of the CMK.

**Table 1.** Physical parameters of red mud

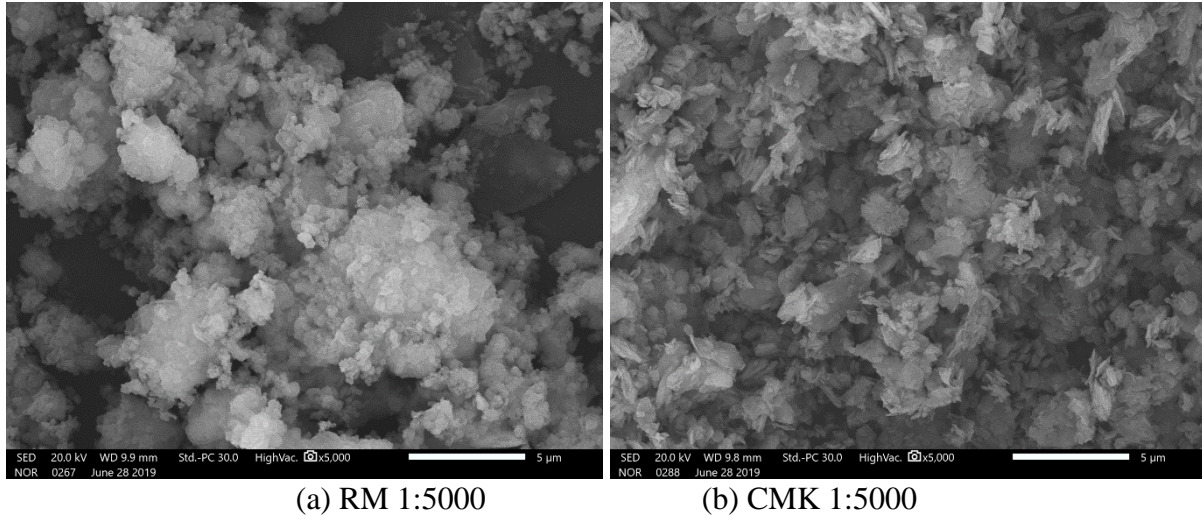
| Particle size/mm |                  |                  |                   | Relative density<br>$D_r$ | Liquid limit<br>$\omega_L/\%$ | Plastic limit<br>$\omega_P/\%$ | Plasticity index<br>$I_P$ |
|------------------|------------------|------------------|-------------------|---------------------------|-------------------------------|--------------------------------|---------------------------|
| 0.075~0.25<br>/% | 0.05~0.075<br>/% | 0.005~0.05<br>/% | $d < 0.005$<br>/% |                           |                               |                                |                           |
| 6.00             | 2.50             | 40.50            | 51.00             | 2.74                      | 36.30                         | 20.25                          | 16.05                     |

**Table 2.** Chemical composition of red mud

| Oxide        | SiO <sub>2</sub> | Al <sub>2</sub> O <sub>3</sub> | Fe <sub>2</sub> O <sub>3</sub> | TiO <sub>2</sub> | CaO   | MgO  | K <sub>2</sub> O | Na <sub>2</sub> O | SO <sub>2</sub> | CO <sub>2</sub> | LOI  |
|--------------|------------------|--------------------------------|--------------------------------|------------------|-------|------|------------------|-------------------|-----------------|-----------------|------|
| Content/wt.% | 21.05            | 27.38                          | 6.42                           | 4.04             | 14.91 | 0.53 | 0.77             | 11.86             | 0.36            | 3.90            | 8.78 |

**Table 3.** Chemical composition of coal metakaolin

| Oxide         | SiO <sub>2</sub> | Al <sub>2</sub> O <sub>3</sub> | Fe <sub>2</sub> O <sub>3</sub> | TiO <sub>2</sub> | CaO  | MgO  | K <sub>2</sub> O | Na <sub>2</sub> O |
|---------------|------------------|--------------------------------|--------------------------------|------------------|------|------|------------------|-------------------|
| Content/wt. % | 52.62            | 45.42                          | 0.45                           | 0.85             | 0.17 | 0.11 | 0.13             | 0.25              |

**Figure 1.** SEM images of RM and CMK

### 2.1.3 Alkali activator

The alkali activator used in the experiment was composed of sodium silicate, sodium hydroxide analytical reagent and distilled water. Sodium silicate was purchased from a building materials production company in Shanxi Province. The main chemical composition of the sodium silicate was SiO<sub>2</sub>, 24.73%; Na<sub>2</sub>O, 8.17%; and H<sub>2</sub>O, 67.10%, and the modulus was 3.12. The sodium hydroxide analytical reagent was pure white granular crystals, purity > 99.0%.

## 2.2 Experimental methods

### 2.2.1 Sample preparation

In this experiment, the ratio of Si/Al was set as 1.2, the mass ratio of RM to CMK was set as 7:3, the water-solid ratio was set as 0.5, and the ratio of Na/Al was set as 0.8, 0.9, 1.0, 1.1, and 1.2. According to the Si/Al, water-solid and different Na/Al ratios, the amounts of sodium silicate, distilled water and sodium hydroxide analytical reagent for the alkali activator solution were calculated, added and stirred. The prepared alkali activator solution was cooled to room temperature. Before the samples were made, it was necessary to supplement the lost water due to the exotherm in the alkali activator solution to ensure that the water-solid ratio was 0.5.

Prior to the sample preparation, the red mud was placed in an oven at 105 °C for 24 h to remove the moisture. During sample preparation, the RM, CMK, and alkali activator solution were portioned as listed in Table 4. All the mixtures were added to a mixer and mixed for 2 min to ensure that the slurry

was stirred evenly; the slurry was then placed in a 40 mm × 40 mm × 40 mm steel mold. The sample surface was scraped flat using a scraper, and the steel mold was wrapped with plastic wrap. Finally, the mold was removed after 24 h. The samples were numbered and placed in a standard curing box. The temperature was controlled to 20±2 °C, the humidity was above 95%, and the curing age was 28 d. In addition, separate samples were kept at each ratio and cut into 15 mm×15 mm×5 mm sections for the SEM analysis.

**Table 4.** Mix proportions

| Specimen | RM content | CMK content | Si/Al | Na/Al | Water-solid ratio |
|----------|------------|-------------|-------|-------|-------------------|
| GP0.8    | 70%        | 30%         | 1.2   | 0.8   | 50%               |
| GP0.9    | 70%        | 30%         | 1.2   | 0.9   | 50%               |
| GP1.0    | 70%        | 30%         | 1.2   | 1.0   | 50%               |
| GP1.1    | 70%        | 30%         | 1.2   | 1.1   | 50%               |
| GP1.2    | 70%        | 30%         | 1.2   | 1.2   | 50%               |

Note: The contents of RM and CMK are the mass ratios, and the sum of the two is the total mass of the solid (100%); Si/Al and Na/Al are the total atomic molar ratios in the reactant.

### 2.2.2 Tests and characterization

A SHT4605 microcomputer controlled electrohydraulic servo universal testing machine was used to test the compressive strength of the RM–CMK geopolymer samples. The maximum loading load was 600 kN, and the loading rate of the press was 2 mm/min.

The EIS of the RM–CMK geopolymer was measured by the CS350 electrochemical workstation's double electrode method. First, copper sheets with a length of 60 mm were pasted on the upper and lower ends of the cube sample. The connecting wires on the copper sheets were connected to the workstation wire clamps. In other words, one end of the wire was connected to the working electrode (WE) wire clamp, and the reference electrode (RE) together with the counter electrode (CE) wire clamp was connected to another end wire to realize the test path. Then, the CS350 electrochemical workstation was opened to test the EIS. The frequency range was set as 10<sup>-2</sup>~10<sup>5</sup> Hz, and the AC amplitude was 10 mV.

A TM-3000 tabletop scanning electron microscope was used to collect microscopic images of the RM–CMK geopolymer samples. The working voltage was 15 kV, and 1000 times and 5000 times magnifications were used.

## 3. RESULTS AND DISCUSSION

### 3.1 Analysis of compressive strength results

Fig. 2 shows the relationship between the compressive strength of the RM–CMK geopolymer and Na/Al at 28 d. With increasing Na/Al ratio, the compressive strength of the RM–CMK geopolymer

first increased and then decreased. When the Na/Al ratio was 1.0, the compressive strength reached the maximum. This is because in the geopolymerization process, when the Na/Al ratio is low, the alkali content is low. There is not enough  $\text{OH}^-$  to ensure that  $\text{Si}^{4+}$  and  $\text{Al}^{3+}$  are completely dissolved from the aluminosilicate, resulting in incomplete depolymerization in the geopolymerization reaction system. With increasing Na/Al ratio, the alkali content increases, and the  $\text{OH}^-$  in solution increases. More  $\text{Si}^{4+}$  and  $\text{Al}^{3+}$  are dissolved from aluminosilicates to participate in the geopolymerization reaction, forming a geopolymer precursor. However, when the Na/Al ratio is too high, the alkali content further increases. The  $\text{Si}^{4+}$  and  $\text{Al}^{3+}$  in the aluminosilicate reach dissolution equilibrium. The free  $\text{Si}^{4+}$  and  $\text{Al}^{3+}$  cannot be dissolved, and the excess  $\text{OH}^-$  in the solution will damage the geopolymer.

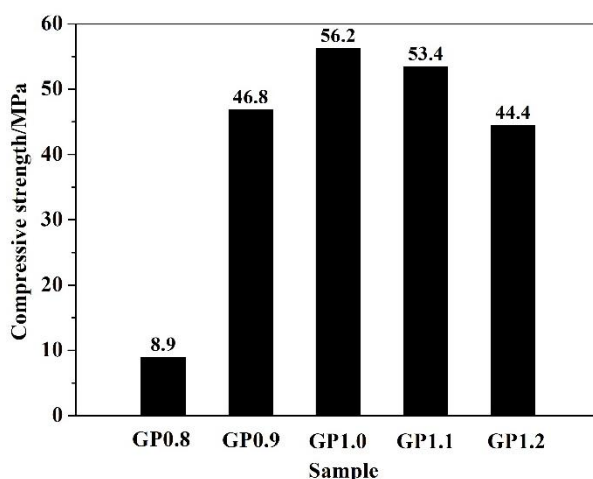


**Figure 2.** Compressive strength of the RM-CMK geopolymer at 28 d

### 3.2 Analysis of EIS results

Fig. 4 shows the Nyquist diagram of the RM-CMK geopolymer at 28 d. The impedance spectra of the RM-CMK geopolymers with different Na/Al exhibited flat capacitive reactance arcs in the high-frequency region and insignificant diffusion curves in the low-frequency region. With increasing Na/Al, the radius of the flat capacitive reactance arc in the high frequency region first increased and then decreased. When Na/Al was 1.0, the radius of the capacitive reactance arc was the largest. The size of the capacitive reactance arc radius represents the difficulty of charge transfer during the electrochemical reaction of the RM-CMK geopolymer. This indicates that the charge transfer resistance of the RM-CMK geopolymer system increases first and then decreases with increasing Na/Al. It was reported that the charge transfer resistance is related to the degree of polymerization of geopolymers [31]. The higher the degree of polymerization is, the denser the inner structure, thus making the process of charge transfer increasingly difficult [32]. This explains why the compressive strength of the RM-CMK geopolymer varies with the Na/Al ratio from the perspective of EIS.

Fig. 5 shows the Bode diagram of the RM-CMK geopolymer at 28 d. From the Bode diagram ( $F-|Z|$ ), it can be seen that the impedance modulus of the whole system first increased and then decreased

with increasing Na/Al. When Na/Al was 1.0, the impedance modulus value reached the maximum. In addition, the Bode diagram ( $F-\theta$ ) shows a peak, indicating that the RM-CMK geopolymer system of different Na/Al exhibited only one capacitive arc. This feature corresponded to the Nyquist diagram. Additionally, the phase angle peak value first increased and then decreased with increasing Na/Al. When Na/Al was 1.0, the phase angle peak value reached the maximum, and the peak frequency was in the frequency domain of  $10^2-10^3$ .

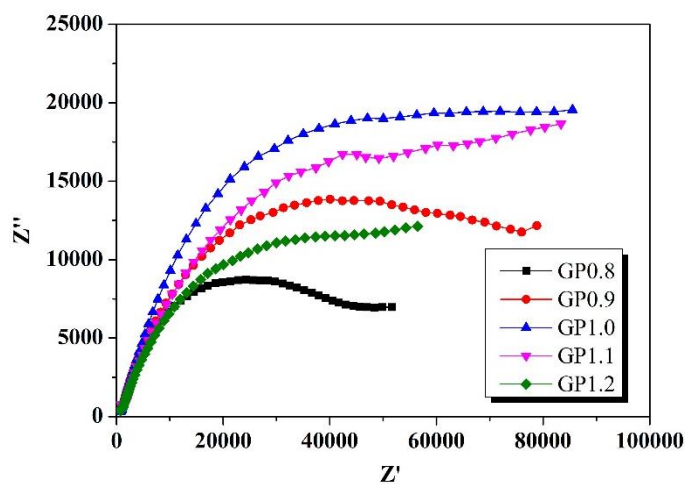


Figure 3. Nyquist diagram of the RM-CMK geopolymer at 28 d

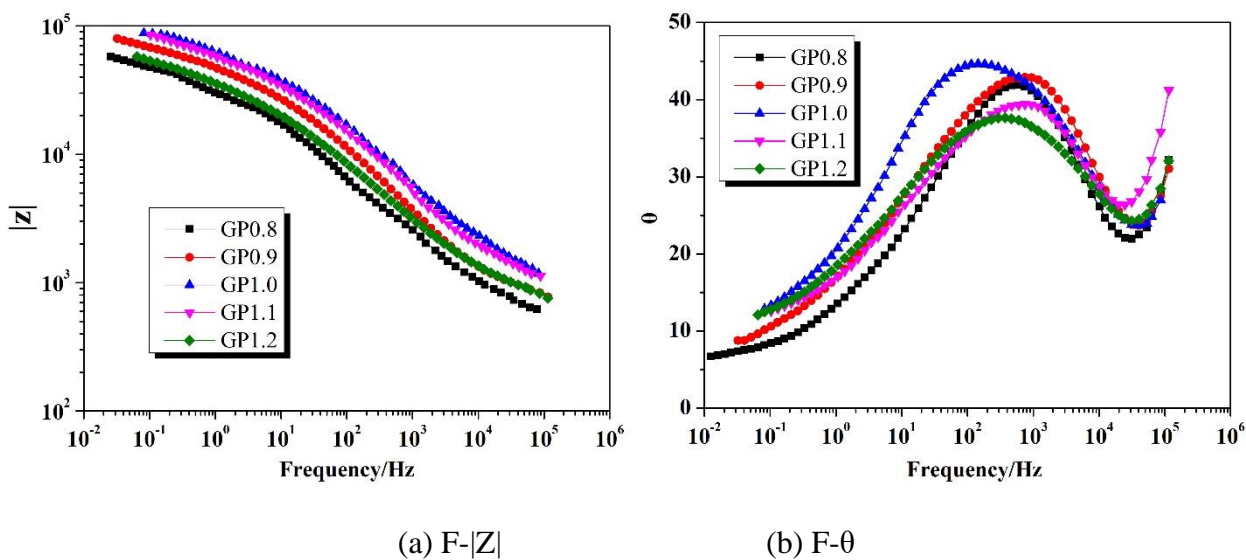


Figure 4. Bode diagram of the RM-CMK geopolymer at 28 d

3.3 Establishment of the equivalent circuit model

When the electrochemical system of a geopolymer material is energized, two main processes are included [33]. One is the process of capacitor charging and discharging when the electrode potential changes; the other process is the Faraday process at a certain electrode potential. Therefore, the electrochemical system of geopolymer materials is usually regarded as composed of two parts: electrodes and electrolytes. The Randles circuit model can be used, and its equivalent circuit model is  $R_e(C(R_{ct}W))$ , as shown in Fig. 5.

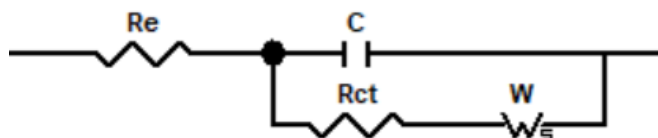


Figure 5. Randles equivalent circuit model

Where  $R_e$  is the total resistance of the geopolymer electrochemical system ( $\Omega \cdot \text{cm}^2$ ),  $C$  is the electric double layer capacitance in the geopolymer gel ( $\text{F}/\text{cm}^2$ ),  $R_{ct}$  is the resistance of charge transfer in the geopolymer gel ( $\Omega \cdot \text{cm}^2$ ), and  $W$  is the diffusion impedance ( $\text{K}\Omega \times \text{m}^2 \times \text{S}^{-1/2}$ ).

In the actual test process, the uneven surface of the samples contacting the electrode was not uniform and smooth. The frequency response characteristics of the electric double layer capacitance of the solid electrode and the pure capacitance  $C$  had different degrees of deviation, resulting in a "dispersion effect". In addition, for geopolymer materials, there is not only an electric double layer capacitance at the electrode and electrolyte interface but also a capacitance caused by a large number of unevenly distributed free charges in the geopolymer gel. Therefore, considering the special gel structure of the RM-CMK geopolymer and the global diffusion of ions in the geopolymerization process, the quasi-Randles equivalent circuit model was adopted in this study, as shown in Fig. 6. The difference between the quasi-Randles model and the Randles model is that the electric double layer capacitor  $C$  in the Randles equivalent circuit is replaced by the constant phase angle element CPE. The total impedance of the equivalent circuit is:

$$Z = R_e + \frac{1}{j\omega C + \frac{1}{R_{ct} + (1-j)\frac{\sigma}{\sqrt{\omega}}}}$$

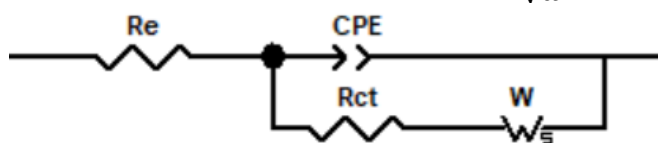


Figure 6. Quasi-Randles equivalent circuit model

### 3.4 Analysis of the equivalent circuit parameters

To further study the electrochemical behavior of the RM–CMK geopolymer, the equivalent circuit was analyzed using ZsimpWin software. Table 5 shows the equivalent circuit parameters.

**Table 5.** Equivalent circuit fitting parameters of the RM–CMK geopolymers

| Specimen | $R_e/\Omega \cdot \text{cm}^2$ | CPE   |            | $R_{ct}/\Omega \cdot \text{cm}^2$ | $W/S \cdot \text{sec}^{0.5} \cdot \text{cm}^{-2}$ |
|----------|--------------------------------|---|------------|-----------------------------------|---|
|          |                                | $CPE_{-T}/S^p \cdot \Omega^{-1} \cdot \text{cm}^{-2}$ | $CPE_{-P}$ |                                   |   |
| GP0.8    | 521.1                          | 2.3E-6  | 0.63       | 8.3E4                             | 1.84E-6   |
| GP0.9    | 540.6                          | 2.7E-6  | 0.65       | 8.2E4                             | 9.40E-5   |
| GP1.0    | 638                            | 3.2E-6  | 0.72       | 6.7E4                             | 7.52E-7   |
| GP1.1    | 527.8                          | 2.7E-6  | 0.68       | 6.2E4                             | 6.56E-5   |
| GP1.2    | 461.4                          | 2.1E-6  | 0.62       | 5.7E4                             | 1.3E-5  |

#### 3.4.1 $R_e$

$R_e$  is the total resistance of the RM–CMK geopolymer electrochemical system. According to the structural parameters,  $R_e$  is inversely proportional to the ion concentration in the closed pores of the geopolymer and the total porosity [34]. The ions in the pore solution of the RM–CMK geopolymer are mainly  $\text{Na}^+$  and  $\text{OH}^-$ . According to the characteristics of geopolymer materials, the geopolymerization reaction is basically completed at the age of 28 d, so the ion concentration changes minimally in the pore solution. At this time, the impedance parameter  $R_e$  is mainly determined by the total porosity. As seen in Table 5,  $R_e$  first increased and then decreased with increasing Na/Al and reached its maximum when Na/Al was 1.0. This is because as the Na/Al ratio increases, the geopolymerization reaction proceeds more fully, and more geopolymer gels are generated. These products fill the pores inside the structure to reduce the total porosity and form a denser structure [35, 36]. However, too high of an alkali content will inhibit the progress of the geopolymerization reaction and damage the internal structure of the geopolymer. Therefore, the total porosity increases, and  $R_e$  decreases. The compressive strength results in section 3.1 and the SEM results in section 3.5 also indicate this analysis.

#### 3.4.2 CPE

CPE is the electric double-layer capacitor in the geopolymer gel.  $CPE_{-T}$  represents the charge of the electric double-layer capacitor, which reflects the capacity of the capacitor to store charge. It is negatively related to the total porosity of the geopolymer. When Na/Al was 1.0, more geopolymer gel was generated, the structure of the geopolymer was the most complete, and the total porosity was the smallest, so the  $CPE_{-T}$  of GP1.0 was the largest.

$CPE_{-P}$  represents the similarity between the normal phase angle element and the pure capacitor. This value is between 0 and 1. When  $CPE_{-P}$  is 0, the CPE represents a pure resistance element; when  $CPE_{-P}$  is 1, the CPE represents a pure capacitance element. Table 5 shows that the equivalent circuit parameter  $CPE_{-P}$  first increased and then decreased with increasing Na/Al. When Na/Al was 1.0,  $CPE_{-P}$

$p$  was the largest. This is because when Na/Al was 1.0, the internal pore structure of the geopolymer was closer to the ideal state of smooth and nonporous, and the structure was denser. Therefore, the CPE of the capacitor was closer to the pure capacitance.

### 3.4.3 $R_{ct}$

$R_{ct}$  is the resistance to charge transfer in the geopolymer gel, which is inversely proportional to the number of free ions in the geopolymer gel. Table 5 shows that the charge transfer resistance  $R_{ct}$  decreased with increasing Na/Al, which occurred because the number of free ions ( $\text{Na}^+$ ,  $^-\text{OSi}(\text{OH})_3$  and  $^-\text{OSi}(\text{OH})\text{O}^-$ ) in the gel increased with increasing Na/Al. This reduced the charge transfer resistance in the geopolymer gel.

### 3.4.4 $W$

$W$  is the diffusion impedance, representing the resistance of the pore solution ions in porous media, which is determined by a combination of various factors. The variation in the porosity of the geopolymer, the ion concentration in the pore solution, the connectivity of the internal pores and the average pore size can all cause variations in  $W$ , so the diffusion impedance  $W$  fluctuates greatly.

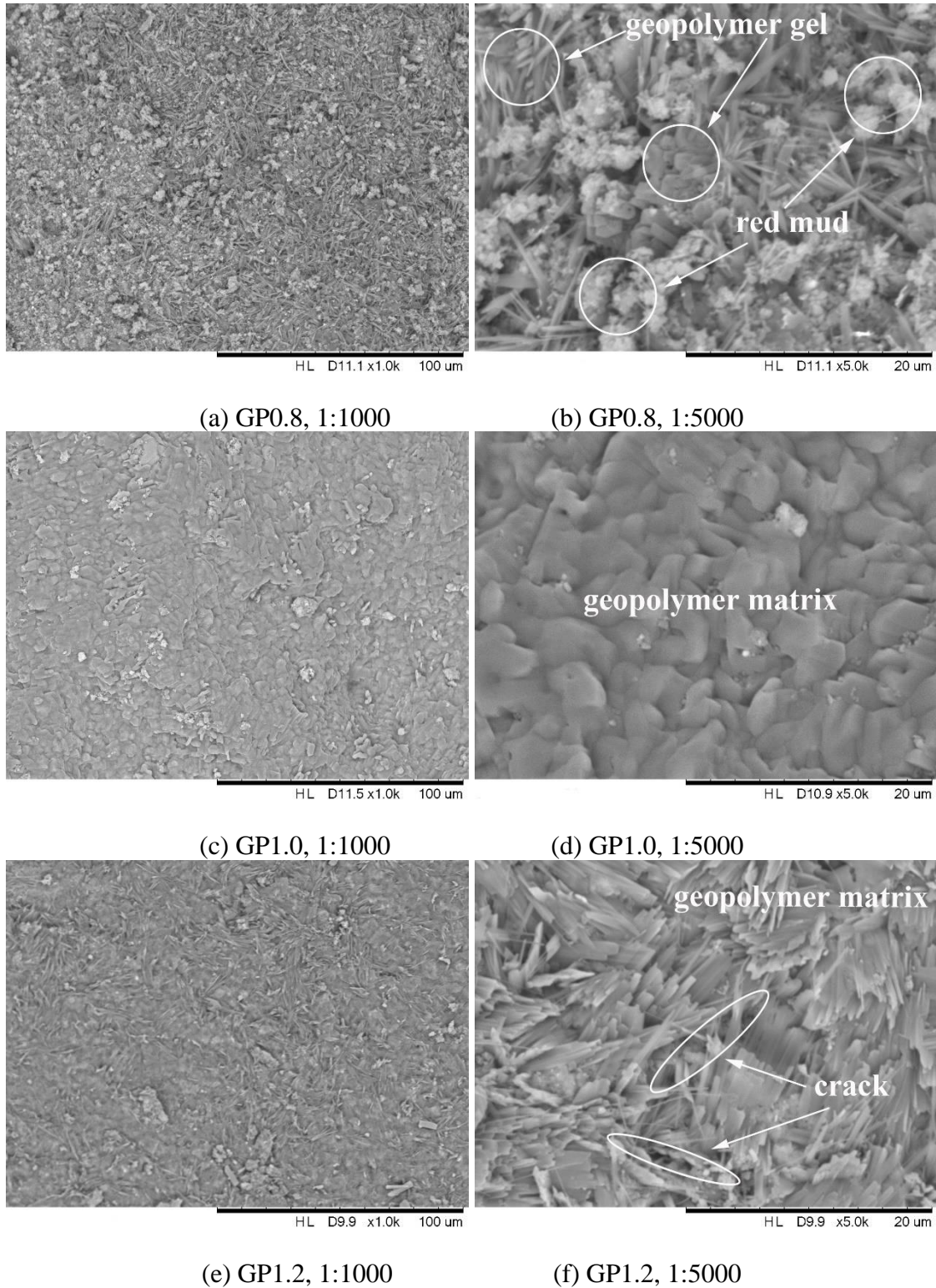
## 3.5 Analysis of SEM results

Fig. 7 shows the SEM images of samples GP0.8, GP1.0 and GP1.2 at 28 d. Fig. 7 (a), (c) and (e) are images at 1000 times magnification, and Fig. 7 (b), (d) and (f) are images at 5000 times magnification.

Fig. 7 (a) shows that the various substances in the GP0.8 hardened slurry were bonded together in particle units. The debris particles were gelled by the cementitious materials to form agglomerate units. The individual particles were mainly cemented by contact, forming a whole with the characteristics of a gelatinous material. Each unit body was loosely arranged, with macropores and relatively high porosity. Fig. 7 (b) shows a local enlarged view of the GP0.8 hardened slurry. As shown in Fig. 7 (b), sheets and clusters of geopolymer gels existed, and the gels were cross-connected to form a whole. Comparison to Fig. 1(a) shows that there were unreacted red mud particles whose surface was covered by a small amount of geopolymer gel. This indicates that when Na/Al was 0.8, the geopolymerization reaction was incomplete, and there was still some unreacted material.

As shown in Fig. 7 (c), the G1.0 hardened slurry became a dense entity. Compared to that of G0.8, its structure was denser, with invisible macropores and high compactness. Fig. 7 (f) shows a local enlarged view of the GP1.0 hardened slurry. The sheet geopolymer gels were bonded together to form a whole geopolymer matrix. Unreacted red mud particles are not seen, indicating that they were fully involved in the reaction. This was why G1.0 exhibited the highest compressive strength, as discussed in section 3.1.

Fig. 7(e) shows that the surface of the G1.2 hardened slurry became uneven, and the geopolymer gels were relatively irregular. Compared to that of G1.0, the dense entity was incomplete, with ravine-like shapes and pores, resulting in a decrease in the compactness. Fig. 7 (f) shows a local enlarged view of the GP1.2 hardened slurry. The flake geopolymer matrix was damaged, and microcracks appeared.



**Figure 7.** SEM images of GP0.8, GP1.0 and GP1.2 at 28 d

#### 4. CONCLUSIONS

In this paper, the compressive strength and electrochemical impedance response of RM–CMK geopolymers with different Na/Al atomic molar ratios were analyzed. The following conclusions were obtained.

(1) The compressive strength of the RM–CMK geopolymer first increases and then decreases with increasing Na/Al. When Na/Al is 1.0, the compressive strength reaches the maximum value of 56.20 MPa at 28 d.

(2) The Nyquist diagram presents flat capacitive reactance arcs in the high-frequency region and insignificant diffusion curves in the low-frequency region. The Bode diagram shows that with increasing Na/Al, the peak values of the impedance modulus and phase angle both first increase and then decrease. When Na/Al is 1.0, the phase angle peak value reaches the maximum, and the peak frequency is in the frequency domain of  $10^2$ - $10^3$ .

(3) The equivalent circuit of the RM–CMK geopolymer electrochemical system is  $R_e(C(R_{ct}W))$ . The equivalent circuit elements include the total resistance of the geopolymer electrochemical system, the electric double layer capacitance in the geopolymer gel, the resistance to charge transfer in the geopolymer gel and the diffusion impedance.

(4) The microstructure of the RM CMK geopolymer changes with increasing Na/Al. When Na/Al is 1.0, the whole geopolymer matrix is formed.

#### ACKNOWLEDGEMENTS

This study was funded by the National Natural Science Foundation of China (No. 51879180, No. 51978438, and No. 41807256), China Scholarship Council (No. 201906930018), Chinese Academy of Sciences (No. Z017003), and Sichuan University of Science and Engineering, Material Corrosion and Protection Key Laboratory of Sichuan Province (No. 2020CL13).

#### References

1. G. Power, M. Gräfe and C. Klauber, *Hydrometallurgy.*, 108 (2011) 33.
2. S. Sushil and V. S. Batra, *Appl. Catal. B.*, 81 (2008) 64.
3. N. Uzinger, Á. r. Anton, K. r. Ö; tvö; s, P. t. Tamá; s and A. Anton, *Environ. Sci. Pollut. Res.*, 22 (2015) 9849.
4. S. Wu, L. Zhu, T. Sun, C. Xu, X. Li and X. Wang, *Met. Min.*, 48 (2019) 38.
5. W. Liu, X. Chen, W. Li, Y. Yu and K. Yan, *J. Clean. Prod.*, 84 (2014) 606.
6. L. Zhang, Y. Gao, J. Huang, S. Chen, Q. Zhang, Y. Chen and J. Fu, *Bull. Chin. Ceramic. Soc.*, 39 (2020) 144.
7. Y. Zhao, H. Wang and Y. Wei, *Mod. Chem. Ind.*, 39 (2019) 55.
8. Q. Liu, X. Yang, P. Zhang and J. Bian, *Acta. Mineral. Sin.*, 22 (2002) 359.
9. Z. Mo, T. Ma and D. Wang, *Bull. Chin. Ceramic. Soc.*, 36 (2017) 110.
10. L. Wang, X. Li, Y. Cheng and X. Bai, *Constr. Build. Mater.*, 166 (2018) 592.
11. L. Wang, X. Li, Y. Cheng, Y. Zhang and X. Bai, *Constr. Build. Mater.*, 186 (2018) 174.
12. S. Wang, Y. Hu, Z. Wang, Y. Zhang, X. Xu, C. Lu, J. Wu and Q. Zhang, *J. Synth. Cryst.*, 47 (2018) 2648.

13. J. Zhang, C. Sun, Z. Cao, W. Fan, Z. Guo and X. Fan, *Inorg. Chem. Ind.*, 48 (2016) 64.
14. S. N. M. Hairi, G. N. L. Jameson, J. J. Rogers and K. J. D. MacKenzie, *J. Mater. Sci.*, 50 (2015) 7713.
15. J. He, Y. Jie, J. Zhang, Y. Yu and G. Zhang, *Cem. Concr. Compos.*, 37 (2013) 108.
16. B. Ilić, V. Radonjanin, M. Malešev, M. Zdujić and A. Mitrović, *Constr. Build. Mater.*, 133 (2017) 243.
17. K. Kaya and S. Soyer-Uzun, *Ceram. Int.*, 42 (2016) 7406.
18. M. Zhang, T. El-Korchi, G. Zhang, J. Liang and M. Tao, *Fuel.*, 134 (2014) 315.
19. P. Han, R. Xie, N. Lin and B. He, *Int. J. Electrochem. Sci.*, 11 (2016) 9491.
20. P. Han, R. Xie, R. Liu, B. He, X. Bai and P. Han, *Int. J. Electrochem. Sci.*, 12 (2017) 7668.
21. F. Ma, R. Xie, P. Han and X. Bai, *Int. J. Electrochem. Sci.*, 13 (2018) 5396.
22. M. Shi and Z. Chen, *J. Chin. Ceram. Soc.*, 24 (1996) 703.
23. H. Wang, L. Hu, P. Cao, B. Lu, J. Tang, F. Shi, J. Yu, H. Li and K. Jin, *Materials.*, 12 (2019) 2815.
24. B. He, P. Han, C. Lu and X. Bai, *Eng. Fail. Anal.*, 58 (2015) 19.
25. B. He, C. Lu, P. Han and X. Bai, *Eng. Fail. Anal.*, 59 (2016) 410.
26. Y. Zhang and M. Shi, *J. Build. Mater.*, 3 (2000) 109.
27. J. Li, R. Xie, P. Han and X. Bai, *Int. J. Electrochem. Sci.*, 15 (2020) 6227.
28. Y. Zhang, P. Han and B. He, *J. Taiyuan Univ. Technol.*, 48 (2017) 55.
29. P. Han, P. Han, R. Xie, B. He and X. Bai, *Int. J. Electrochem. Sci.*, 13 (2018) 8694.
30. P. Han, P. Han, Y. Yan and X. Bai, *Int. J. Electrochem. Sci.*, 13 (2018) 10548.
31. Y. Chen, S. Lin, J. Wang, S. Hsu and C. M. Ma, *J. Electrochem. Soc.*, 165 (2018) A3029.
32. Z. Xu, *J. Chin. Ceram. Soc.*, 22 (1994) 173.
33. P. Payakaniti, S. Pinitsoontorn, P. Thongbai, V. Amornkitbamrung and P. Chindaprasirt, *Constr. Build. Mater.*, 135 (2017) 164.
34. S. Hanjitsuwan, S. Hunpratub, P. Thongbai, S. Maensiri, V. Sata and P. Chindaprasirt, *Cem. Concr. Compos.*, 45 (2014) 9.
35. M. Shi and Z. Chen, *J. Build. Mater.*, 1 (1998) 30.
36. M. Shi, X. Zhang, P. Li and L. Jiang, *Bull. Chin. Ceramic. Soc.*, 18 (1999) 14.